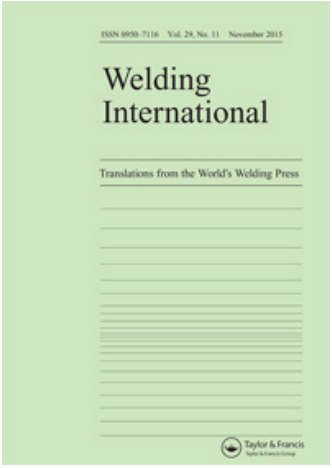

Welding International
Publication details, including instructions for authors and subscription information:
http://www.tandfonline.com/loi/twld20

Effect of heat input on the Fe-based nanostructured weld overlay

Agustín Gualco[a], Hernán G. Svoboda[bc] & Estela S. Surian[ad]

[a] Faculty of Engineering, National University of Lomas de Zamora, Buenos Aires, Argentina

[b] Laboratory of Materials and Structures, Department of Mechanical Engineering, INTECIN, Faculty of Engineering, University of Buenos Aires, Buenos Aires, Argentina

[c] National Council of Scientific and Technical Research, Buenos Aires, Argentina

[d] San Nicolas Regional Faculty, DEYTEMA - Centre of Development and Technology of Materials, National Technological University, San-Nicolas, Argentina

Published online: 18 Mar 2015.

To cite this article: Agustín Gualco, Hernán G. Svoboda & Estela S. Surian (2015) Effect of heat input on the Fe-based nanostructured weld overlay, Welding International, 29:11, 847-855, DOI: 10.1080/09507116.2014.932992

To link to this article: http://dx.doi.org/10.1080/09507116.2014.932992

Welding International, 2015
Vol. 29, No. 11, 847–855, http://dx.doi.org/10.1080/09507116.2014.932992
Selected from *Soldagem & Inspeção* 2013 18(4) 329–338

Effect of heat input on the Fe-based nanostructured weld overlay

Agustín Gualco[a,*], Hernán G. Svoboda[b,c] and Estela S. Surian[a,d]

[a]*Faculty of Engineering, National University of Lomas de Zamora, Buenos Aires, Argentina;* [b]*Laboratory of Materials and Structures, Department of Mechanical Engineering, INTECIN, Faculty of Engineering, University of Buenos Aires, Buenos Aires, Argentina;* [c]*National Council of Scientific and Technical Research, Buenos Aires, Argentina;* [d]*San Nicolas Regional Faculty, DEYTEMA – Centre of Development and Technology of Materials, National Technological University, San-Nicolas, Argentina*

In the last few years, several welding consumables have been developed that deposit hard iron-based nanostructured alloy coverings with high resistance to abrasive wear. The erosive and abrasive wear resistances are mainly controlled by the chemical composition and the microstructure. In turn, the microstructure of the deposited metal can show variations with the used welding procedure, particularly in relation to the heat input. The operating parameters that define the heat input (voltage, current and welding speed) affect aspects such as bead geometry (wide, penetration and reinforcement) and dilution with the base material. The purpose of this article is to study the effect of heat input on the geometric characteristics of the bead, the dilution and the microstructural evolution of a nanostructured iron-based alloy deposited by FCAW. Several samples with heat input between 0.5 and 3.5 kJ/mm were welded. A dimensional study was carried out for each welded coupon, the chemical composition was analysed and the microstructure was characterized using optical and electronic scanning microscopy and X-ray diffraction. Microhardness, crystallite size and degree of dilution were also measured. Great influence in these conditions in the process was observed about the geometry of the bead. The dilution varied between 30% and 40%; microhardness of the deposit was found between 800 and 870 HV1, and the size of the crystallite varies between 105 and 130 nm, depending on process variables used. The highest hardnesses and the lowest crystallite sizes were obtained with the lowest heat input, associated with a lower dilution.

Keywords: hard coverings; nanomaterials; heat input; microstructure

1. Introduction

The technology of materials for surface coverings has experienced significant progress in the last few years, continuously developing specific coatings for particular needs. In this aspect, the systematic study of the consumables and procedures of welding for the application of hard coatings is of great interest for the optimization of the design of said consumables and for the evaluation and reshaping of the mentioned welding procedures. In this context, the heat input, the composition of the protective gas, the temperature of preheating and between passes and the post-welding thermal treatment are some of the most relevant variables in the welding procedure [1,2].

The deposits under study are of a high hardness, with precipitates of complex, ultra-hard boro-carbides, carbides and borides, distributed in a nanostructured α-ferritic matrix. During cooling of the melted metal, although the random movement of the atoms generates dispersed and non-ordered groups, during solidification, the majority settle in a predetermined, regular, crystalline structure. Unusually, under very rapid cooling, certain alloys can be 'frozen', retaining their liquid atomic arrangement, due to insufficient time for their 'ordering'; in this way, a super-cooled vitreous structure is obtained having unusual properties. This 'rapid solidification technology' is used for the generation of metallic layers on a microscopic scale, which combine high resistance, elastic modulus and resistance to corrosion. However, this technology is not adequate to produce amorphous structures on a macroscopic scale in which the useful thickness of the weld overlay is not required in microns, but in millimetres. For this latter case, it was discovered that if various and different elements with very different atomic radii are melted together, on solidifying, the resulting alloy presents great difficulties for nuclear power and grows according to the normal crystalline regulation and what is obtained are grains of a nanometric size in a 'nano alloy' microstructure [3], a state of atomic aggregate between the crystalline order and the complete disorder characteristic of the liquid state. The materials obtained in this way which are suitable for deposits for welding have exceptional resistance to abrasion and erosion; deposits of a single layer with extremely high hardnesses (70 HRc), low friction coefficient without lubrication and soft surface beads.

From the recent advances in the area of welding, tubular wires have been developed which allow iron alloys with a nanostructured α-ferritic matrix with precipitated carbides and borides [2,3]. These materials have an increased hardness associated with the extremely small size of the crystallite of the matrix, of the order 30–50 nm. It must be clarified that crystallite is a solid composed of atoms ordered in a periodic pattern in three dimensions, whose measurement is implemented with X-ray diffraction (DRX). If said measurement had been carried out by transmission electron microscopy, it would be designated as a grain [4]. Furthermore, in general, these materials have ultra-hard precipitates such as niobium, boron (or chrome boro-carbides) or tungsten, which improve the

*Corresponding author. Email: agustingualco@yahoo.com.ar

resistance to abrasive wear. They are applied to new surfaces or to worn pieces of equipment, having specific properties such as being able to be resistant to abrasive and adhesive wear, to erosion, to corrosion, to heat and their combinations [1]. Based on recent statistics, it is estimated that 50–60% of elements in equipment are worn due to erosion and/or abrasion (of low pressure, high pressure, in the dry or damp) [1,2,5] for which its application presents a strong impact on the lifespan of the components.

The resistance to the abrasive wear of deposits obtained by FCAW depends on many factors, but principally the chemical composition and the microstructure are those which define its properties [2]. In turn, the heat input, which depends on the welding speed, the current and the arc voltage, and which defines the thermal cycle, strongly influences the solidification structure of the deposited material and furthermore controls the shape of the melting line, the depth of penetration and the dilution of the deposit. Previous studies [6–8] have shown that an increase in the heat input produces changes in the chemical composition of the deposited metal, in its microstructure and an increase of the thermal effect between passes, and, for that matter, variations in the final mechanical properties of the deposit. In nanostructured alloy deposits, it has been observed that the dilution is that which has a greater effect on the structural characteristics of these materials, due to which the chemical composition is that which principally defines the size of the crystallite of the matrix [9]. However, the information available about welding the new Fe-based multicomponent systems is scarce, due to which it is necessary to get to know how different thermal inputs modify the chemical composition and the structural evolution, together with other aspects of the deposited metal. The purpose of the following article is to study the influence of the thermal input on the geometry of the bead, the dilution, the structure and the microhardness of the Fe-based nanostructured alloy deposits.

2. Materials and methods

2.1 Welding

The consumable used was a tubular wire of 1.6 mm diameter, deposited by means of the semiautomatic welding process with gaseous protection, using Ar–20% CO_2 with a gaseous flow rate of 18 l/min and a free longitude of the wire of 20 mm in all cases, in mechanized form, using a Miggytrac device. In Table 1 is shown the nominal chemical composition of deposited metal according to the manufacturer.

For the purpose of being able to evaluate the effect of the heat input on the bead properties, eight coupons with

Table 1. Chemical composition of the pure filler metal (% by weight).

C	Mn	Si	Cr	Nb	B	Fe
<2	<2	<2	<18	<6	<6	Bal.

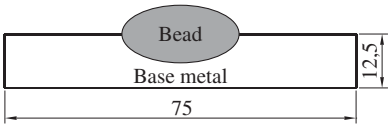

Figure 1. Diagram of the bead (mm).

two levels of electrical power and four welding speeds were welded. The parameters were chosen with the purpose of being able to compare extreme situations of thermal input and others which had the same or similar heat input but obtained via different electrical powers and forward speeds.

A welding bead was deposited in a flat position, on eight base sheets of 150 mm × 75 mm × 12.5 mm made of carbon steel of the type SAE 1010, as is shown schematically in Figure 1. The welding parameters used can be seen in Table 2, as well as the identification used and the heat input calculated in each case. The different test pieces are grouped into two series denoted with the letters L (low) and H (high), associated with the electrical power used; the number added to the letter corresponds to the welding speed used.

According to the chosen welding parameters, two pairs of test pieces were welded with different power and welding speed, but with similar or the same heat input. The test pieces are H7 and L3, with 1.5 and 1.7 kJ/mm of heat input respectively, and on the other hand, H10 and L5, both with 1.0 kJ/mm.

After welding the different test pieces, a visual inspection was carried out analysing the surface aspect and the presence of macroscopic surface defects.

On the other hand, for the purpose of determining the chemical composition of the free dilution deposit, a pure filler coupon was welded for chemical analysis (Figure 2). The sequence of the same was of three layers with four, three and two beads in a flat position. The welding parameters used were of 300 A, 35 V and 5 mm/s of forward speed.

2.2 Chemical analysis and microstructural characterization

Cross sections were extracted from each of the test pieces, which were prepared for metallographic observation. Chemical composition measurements were carried out on these by means of energy dispersive X-ray spectrometry (EDS). The boron was measured by means of the moisture path technique. Measurements of the Cr and Nb were carried

Table 2. Welding parameters.

Identification	Arc voltage (V)	Current intensity (A)	Electrical power (kW)	Welding speed (mm/s)	Heat input (kJ/mm)
L3	25	200	5.0	3	1.7
L5	25	200	5.0	5	1.0
L7	25	200	5.0	7	0.7
L10	25	200	5.0	10	0.5
H3	35	300	10.5	3	3.5
H5	35	300	10.5	5	2.1
H7	35	300	10.5	7	1.5
H10	35	300	10.5	10	1.0

Note: L, low electrical power; H, high electrical power.

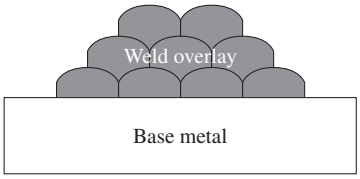

Figure 2. Diagram of the pure filler coupon.

out with EDS for cross sections at 1 mm from the free surface of the bead and at 1 mm from the melting line. The dimensions of the beads, width, penetration and mounting, were measured by means of image analysis software. The microstructure was characterized by means of a scanning electron microscope (SEM). Using the cross sections, Vickers microhardness (HV1) was measured over 1 mm of the surface, in five areas, averaging the obtained values. The microhardness was also taken using the phases with $HV_{0.05}$.

Using the surface of each bead, DRX was carried out in the striped area of Figure 3. The equipment used was a RIGAKY, with Cu K-α radiation between 35° and 95°, which a scanning speed of 1°/min. From the spectra obtained, the present phases were analysed and the size of the crystallite of the α-ferritic phase was determined, using the Scherrer formula [10]:

$$\beta = \frac{0.9\lambda}{D\cos\theta},$$

where β is the average width of the peak (radians), λ is the longitude of the wave (Å), θ is the Bragg angle (radians) and D is the size of the crystallite (nm).

The methodology used for the quantification of the phases by XRD was by means of data bases and RIR (reference intensity ratios) factors [11]. The software used allows quantitative analyses to be made using methods of nonlinear least squares for the complete profile of the diagram. The sampling is carried out with the normalized RIR method.

3. Results and discussion

3.1 Visual inspection

In Figure 4, the photos of the surface aspect of the deposited beads can be seen by means of the different operative configurations studied.

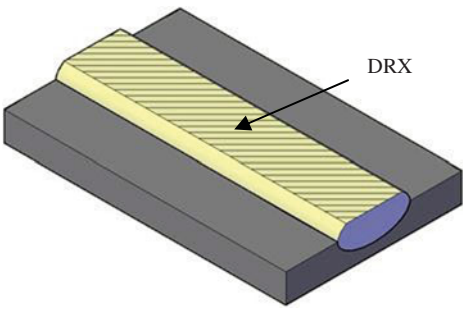

Figure 3. Diagram of the measurement area of DRX.

It was observed that in all of the welded test pieces, the levels of the sprinklings and of the generation of slag were low. Furthermore, the beads had a good surface finish. In the majority of them were found fissures which were generated during the cooling of the welded bead, produced by the release of tension, typical in these materials.

The width of the beads increases with the heat input. The two sets of welded test pieces, H7–L3 and H10–L5, with similar or the same heat input and different operative parameters, had similar surface aspect.

3.2 Macrography and dimension analysis of the beads

In Figure 5, the macrographies of the different cross sections of the coupons are shown. Both the base metal and the deposit can be seen and the absence of the macroscopic defects, such as pores and inclusions, is shown.

In Table 3, the measured values for width, penetration and mounting are presented for each of the deposited beads.

It can be seen that the geometry of the bead is strongly affected by the process parameters used. In Figure 6, the evolution of the width, penetration and the mounting of the bead is depicted with the welding speed, with each L and H series separately, for the purpose of seeing the effect of the power used.

The increase in the welding speed produced a decrease in the width of the bead and of the penetration, for both series. Furthermore, on decreasing the electrical power, the penetration and the width of the bead also decreased, consistent with that which was expected. With respect to the mounting, it was observed that it was better for the welded test pieces with less electrical power. This was associated with an increase in the voltage, producing a flattening of the bead, and for that matter a decrease in the mounting. The speed slightly modified the height of the bead, and this was related to the lowest volume of the input material.

In turn, for the conditions with the same thermal input (L3 similar to H7 = 1.5–1.7 kJ/mm and L5 = H10 = 1.0 kJ/mm), the geometry of the bead shows variation. In the case of 1.5–1.7 kJ/mm, the test piece had a significantly smaller width, with a penetration that is slightly greater and a mounting that is strongly greater than test piece H7. In the case of 1 kJ/mm, the test piece had double the value for mounting, with a width and penetration that was practically the same. These considerations make it clear that the geometry of the deposited bead does not remain defined by the thermal input, but that the variables that define said input should be considered independently. This aspect is especially relevant in the case of the welding of weld overlay, given that the geometric aspects of the deposit can affect the dilution and the surface covered, questions which define the quantity of layers required and, definitively, aspects of quality and the cost of a given covering.

Based on the geometries of the beads, the volumetric dilution of each sample [2] was calculated by means of

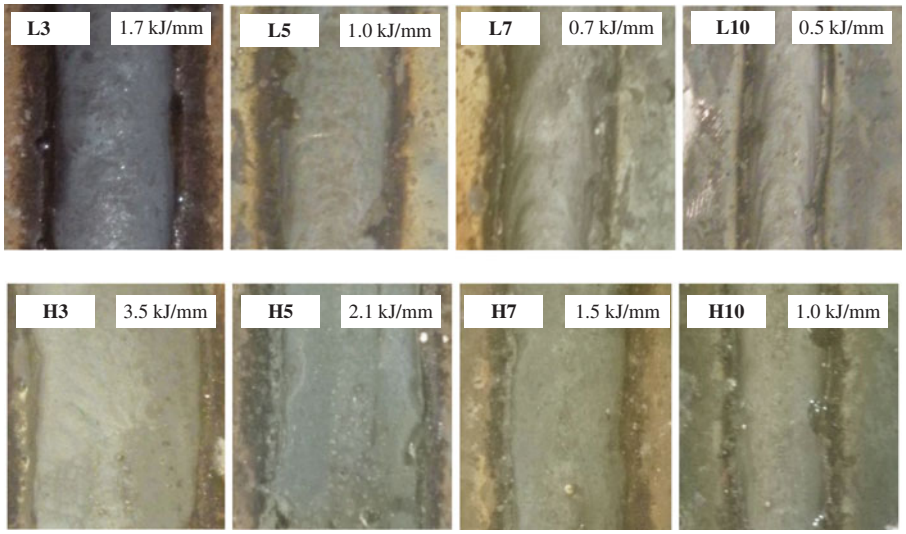

Figure 4. Top view of the welded beads (1 ×).

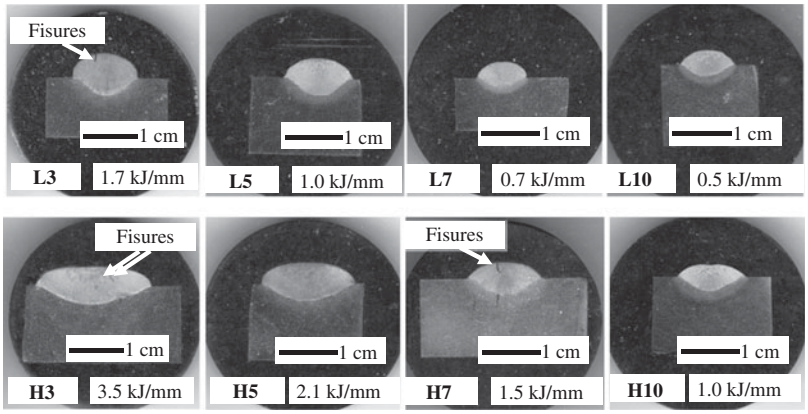

Figure 5. Macrostructure of the welded test pieces.

image analysis software. The results are presented in Table 4.

The percentage dilution varied between 30% and 38% for the different welding conditions. Considering that the thermal input was varied to a factor of 7, the effect of said thermal input on the dilution can be considered low. Even though the variations are small, the welding samples with greater electrical power showed the greater dilution values. This was related to the greater current applied which produces greater penetration. Furthermore, it is observed that the increase in the welding speed produces a decrease in the dilution, which, in a similar way, was associated with the decrease in the penetration with the welding speed. Additionally, it can be seen that for the conditions with similar thermal input (L3/H7 and L5/H10), variation in the dilution was not observed.

3.3 *Chemical composition*

In Table 5 is shown the result of the chemical analysis obtained for the pure filler metal coupon.

The deposited material had a high concentration of alloyed elements within the Fe–(Nb,Cr)–(C,B) system. The chemical composition fulfils the regulations for the formation of nanostructures, which are: that the system has multiple components, with at least three alloyed elements, a difference of atomic radius between the elements which make up the alloyed system which is greater than 12% and that the heat of mixing between its three main elements is negative [12–14]. These characteristics produce great difficulties for nucleation and the growth of layers of regular atoms, producing crystals of nanometric size.

For the purpose of evaluating the chemical homogeneity within the bead, measurements of the Cr and Nb were carried out with EDS with cross sections at 1 mm from the

Table 3. Measured width, penetration and mounting for the different deposited beads.

Test piece	L3	L5	L7	L10	H3	H5	H7	H10
Heat input (kJ/mm)	1.7	1.0	0.7	0.5	3.5	2.1	1.5	1.0
Forward speed (mm/s)	3	5	7	10	3	5	7	10
Width of bead (mm)	12	11	9.5	8.2	18	16	14	11
Penetration (mm)	3.1	2.7	2.3	2.0	3.5	3.2	2.8	2.6
Mounting (mm)	4.0	3.9	3.7	3.2	2.8	2.6	2.5	2.0

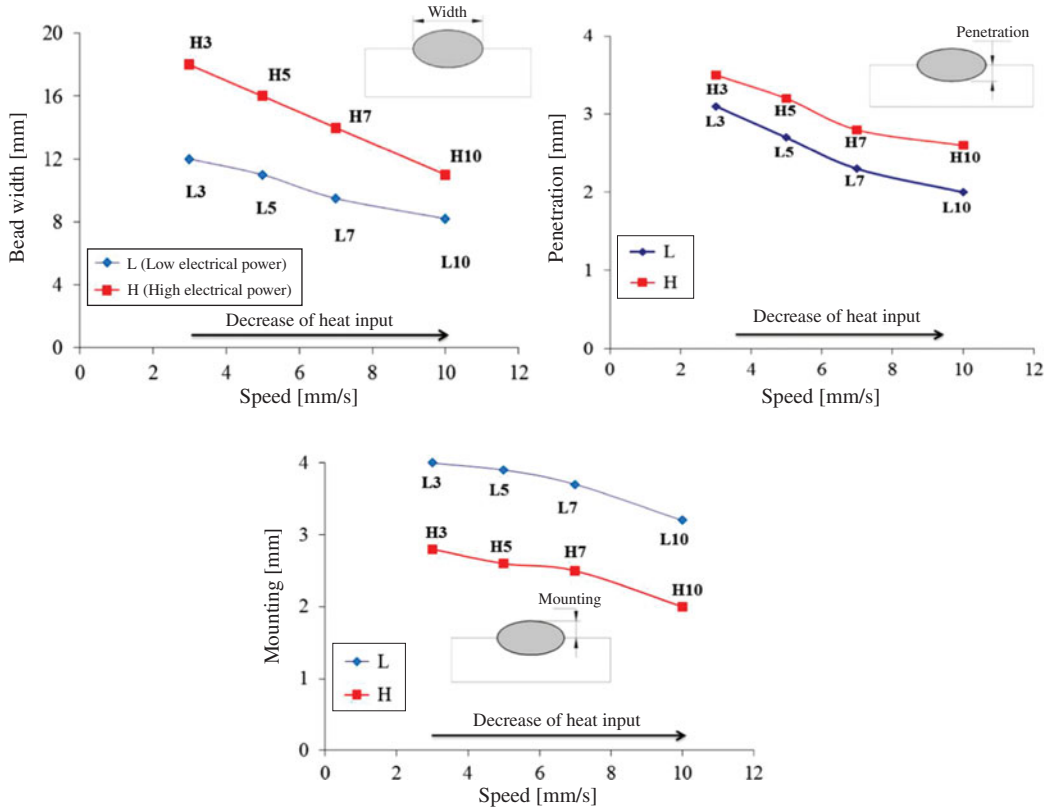

Figure 6. Width of the bead and penetration of all the welded samples.

free surface of the bead and at 1 mm from the melting line. In these determinations, no significant differences were found between the two values (<5%), due to which it can be considered that the chemical composition within the bead was homogeneous. The results obtained are presented in Table 6.

It is observed that the increase in the welding speed generated an increase in the concentration of Cr and Nb in the deposit. Additionally, on decreasing the thermal input, a high concentration of Cr and Nb was observed. This was related with the level of dilution of the filler with the base metal, which depends on the parameters of the process used [2], and with a greater oxidation of elements in the electrical arc on increasing the thermal input. In the samples with similar or the same thermal input and different parameters, the concentration of said elements was similar.

From the data obtained concerning the pure filler metal composition, the base material and the deposited beads, the average values of dilution were calculated for each test piece. In Figure 7, the results obtained are shown, together with the volumetric dilution values determined in Table 2.

As was mentioned previously, it was observed that on increasing the heat input, the dilution increased. This is consistent with that observed in the penetration graphics and in the cross sections.

The dilution values obtained for the two techniques are very similar, demonstrating the same tendency, even though the volumetric dilution presented slightly lower values. This could be associated with a greater local solidification time occurring on increasing the thermal input, due to which the oxidation effect in the arc could reduce the concentration of the elements of low oxidation power in the deposit [15] generating in this way greater values of chemical dilution.

In this sense, the validation found of the measurement techniques of the volumetric dilution with respect to the chemical dilution is interesting as the first is a simple and quick technique. Additionally, the fact that the dilution has been found between 30% and 40% for such wide variations of thermal input is also a relevant piece of information given the importance of the chemical composition in the formation of nanostructured materials.

Table 4. Volumetric dilution for the different welding conditions.

Test piece	L3	L5	L7	L10	H3	H5	H7	H10
Heat input (kJ/mm)	1.7	1.0	0.7	0.5	3.5	2.1	1.5	1.0
Dilution (%)	35	34	32	30	38	36	36	35

Table 5. Chemical composition of the pure filler metal (% by weight).

C	Mn	Si	Cr	Nb	B	Fe
0.99	0.22	1.02	16.8	4.6	4.6	Bal.

Table 6. Concentration of Cr and Nb (% by weight) in the different deposited beads.

Test piece	L3	L5	L7	L10	H3	H5	H7	H10
Heat input (kJ/mm)	1.7	1.0	0.7	0.5	3.5	2.1	1.5	1.0
Cr	10.7	10.8	11.3	11.5	10	10.4	10.6	10.9
Nb	3.4	3.5	3.6	3.9	3.3	3.5	3.5	3.6

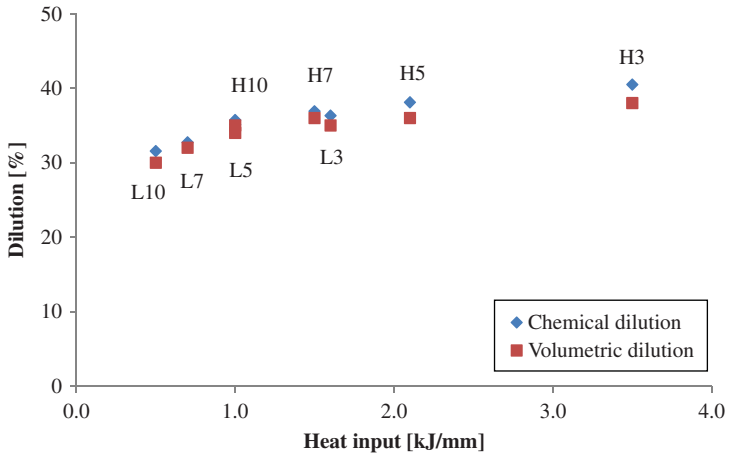

Figure 7. Relation between the chemical and volumetric dilutions and the heat input of all of the beads.

3.4 *Microstructural characterization*

In Figure 8, the DRX spectra obtained are shown for all of the conditions. It can be seen that the structure was formed principally by α-Fe (56% (H3) at 49% (L10)) and boro-carbides ($M_7(BC)_3$, $M_{23}(BC)_6$) (38% (H3) at 44% (L10)), also detecting the presence of a low fraction of γ-Fe and niobium carbide (NbC; less than 1%) [11].

Additionally, from these spectra, the size of the crystallite of the α-Fe, which varied from 105 nm for L10 (0.5 kJ/mm) to 130 nm for H3 (3.5 kJ/mm), the minimum and maximum heat inputs used were determined, observing an increase in the thermal input. These variations could be related to the total percentage of alloyed elements [14] which decrease with the increase of heat input and the lower cooling speed associated with a greater heat input, which could affect the growth of the nanocrystals.

Regarding microscopic observation, in Figure 9 can be seen SEM images of the microstructures obtained for different welding conditions.

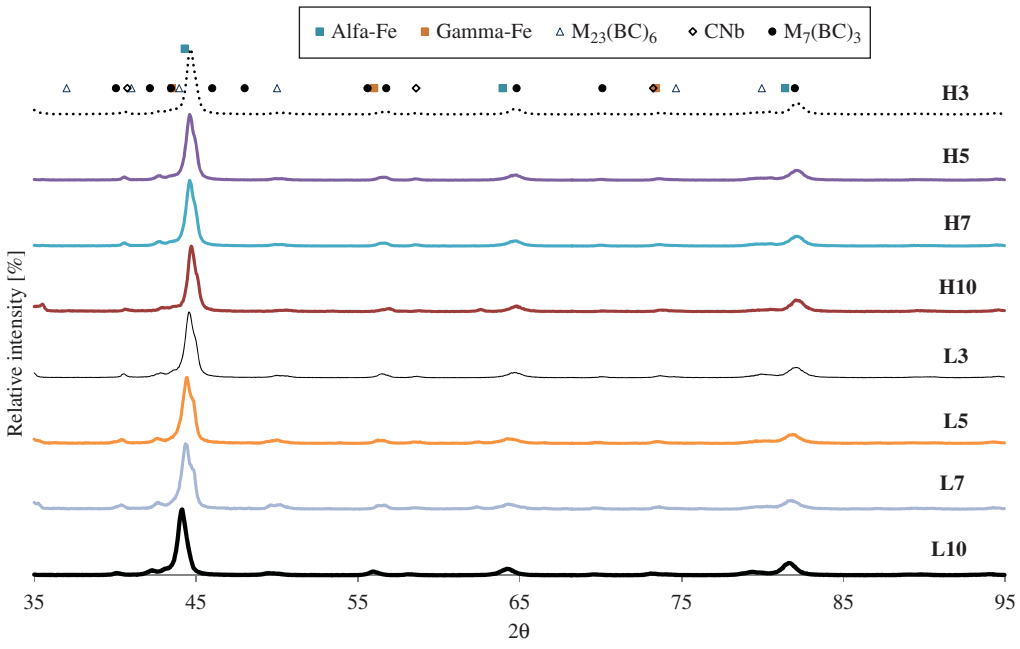

Figure 8. XRD spectra of all of the conditions.

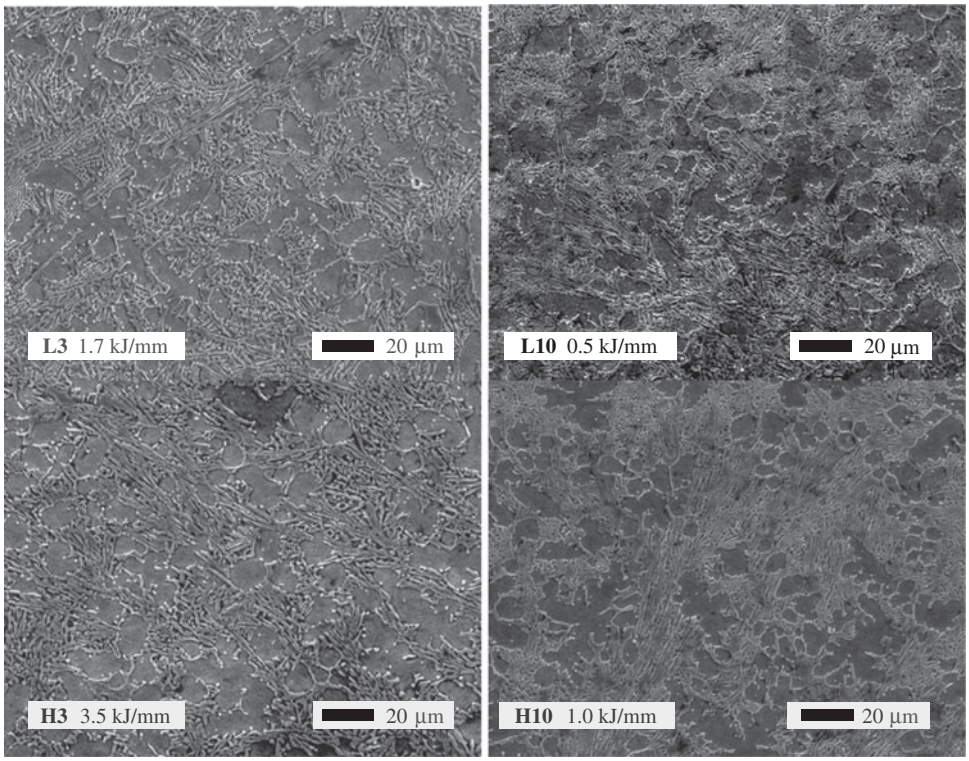

Figure 9. SEM micrographies of the test pieces H3, H10, L3 and L10.

A pattern of dendritic segregation is observed, which becomes finer due to the decrease of the thermal input. In the interdendritic area, a eutectic laminar/globular structure can be seen, which also refines on decrease of the thermal input. This structure was composed of α-Fe and boro-carbides, consistent with that which was determined in the XRD spectra. In Figure 10, a detail of said area in the test piece H3 is shown. The interdendritic area indicated as A shows a greater concentration of alloyed elements (13% Cr, 2% Nb), whilst in area B the concentration of Cr and Nb decreased (7% Cr and 1% Nb). This greater concentration of alloys in zone A is consistent with the interdendritic placement of said area, which was enriched in said elements due to corresponding with the last liquid to solidify. It was observed that the eutectic fraction increased on decrease of the heat input.

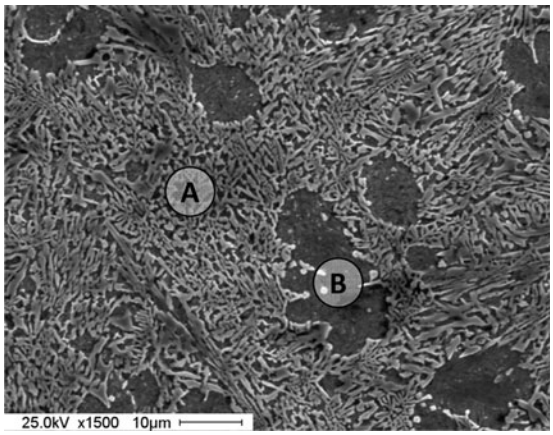

Figure 10. Detail of the microstructure of the H3 coupon.

3.5 *Microhardness testing*

In Table 7, the results of the microhardness testing are observed, averaging at least three measurements. It can be seen that the values vary between 806 and 862 HV, being consistent with that which is expected for this material [12,16]. For the test pieces with similar thermal input, equivalent hardnesses were obtained. An increase in the microhardness was observed on decreasing the thermal input. This increase was associated with the smaller size of the crystallite and greater content of the elements in the product solution of the lower dilution. In Figure 11, the microhardness is depicted using the size of the crystallites and the heat input.

Additionally, the microhardness in both observed microconstituents was determined (α-Fe matrix and eutectic structure). The average values determined were 749 $HV_{0.05}$ for the α-Fe matrix and 949 $HV_{0.05}$ for the globular structure. Given that the fraction of the softer α-Fe phase increase with the thermal input, this could explain the decrease in the hardness with the heat input. Additionally, as was mentioned before, on decreasing the thermal input, a decrease in the size of the crystallite of the α-Fe matrix and a decrease in the dilution of the resulting increase of the alloyed elements is produced, which could explain the increase in hardness observed. The existence of a relationship between the size of the crystallite and the microhardness has been reported previously in the literature for nanostructured materials [16–20].

Table 7. Microhardness (HV1 kg).

Test piece	L3	L5	L7	L10	H3	H5	H7	H10
Heat input (kJ/mm)	1.7	1.0	0.7	0.5	3.5	2.1	1.5	1.0
Dilution (%)	35	34	32	30	38	36	36	35
Hardness (HV)	838 ± 5	842 ± 6	850 ± 5	862 ± 4	806 ± 6	836 ± 7	841 ± 8	847 ± 5

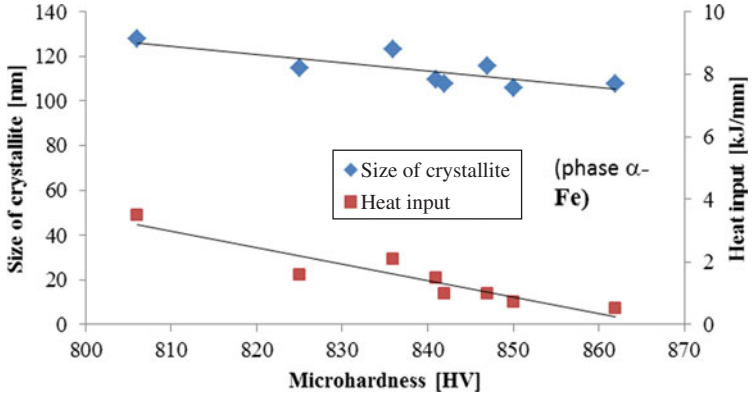

Figure 11. Relation between size of crystallite, microhardness and heat input for the conditions.

4. Conclusions

In the present thesis, the effect of the welding parameters on the characteristics of the deposits obtained in an Fe-based nanostructured alloy deposited by means of a tubular wire under gaseous protection with thermal inputs between 0.5 and 3.5 kJ/mm was evaluated.

It is concluded that:

- All of the welded test pieces have a good surface finish and low levels of scattering and slag. The majority of this fissured during cooling.
- The width of the bead, the penetration and the mounting of the beads deposited increased with heat input. For the same heat input, it was observed that the geometry of the beads was different in terms of the parameters used, principally the mounting, which decreased with the increase of the electrical power.
- The dilution measured by means of the variation of the chemical composition and of the volumetric analysis presented similar values, validating the technique of volumetric determination which is quicker and more simple. The material deposited presented a dilution of 30% for the lowest thermal input (0.5 kJ/mm) and of 38% for the greatest thermal input (3.5 kJ/mm).
- The microstructure was formed by a matrix of α-Fe boro-carbides ($M_7(BC)_3$, $M_{23}(BC)_6$), with low fractions of γ-Fe and CNb. A eutectic structure was observed, formed by α-Fe boro-carbides. The fraction of this structure decreased with the increase of the thermal input.
- The size of the crystallite of the α-Fe matrix increased with the thermal input from 106 to 130 nm. This increase of the crystallite size could be due to the decrease of the alloy content of the deposit on increase of the heat input.
- The hardness increased with the decrease of the thermal input from 806 to 862 HV for the extreme values of heat input analysed. This increase of the microhardness is associated with hardening due to solid solution and with the smaller size of the crystallite of the α-Fe matrix, and with the increase of the quantity of the eutectic structure of greater hardness.

Acknowledgements

The authors give thanks to Eutectic-Conarco Argentina for the provision of the consumable used, to Air Liquide Argentina for the donation of the welding gases, to Eutectic-USA for the implementation of the chemical analysis, to the Laboratorio de Microscopía Electrónica de Inti – Mecánica for the implantation of the scanning electronic microscopy and to Apuenfi (Association of Entrepreneur Lecturers in the Area of Mechanics of the Faculty of Engineering – University of Lomas de Zamora) for the economic support for the present project.

References

1. Linnert GE. Welding metallurgy carbon and alloy steels. 4th ed. Miami (FL): AWS; 1994.
2. Merrick S, Kotecki D, Wu J. Materials and applications. Part 2: welding handbook. American Welding Society; 1998.
3. Heath G. Nanotechnology and welding – actual and possible future applications. In: Proceedings of the Castolin-Eutectic seminar; Brussels, Belgium; 2006. p. 25.
4. Allen S, Edwin T. The structure of materials. New York: Wiley; 1999.
5. Klimpel A, Janicki D. A study of worn wear plates of fan blades of steel mill fumes suction system. In: Proceedings of the 13th scientific international conference. Achievements in mechanical and materials engineering (AMME); 2005; Gliwice, Polonia. 307–310.

6. Evans GM. The effect of heat input on the microstructure and properties of C-Mn all-weld-metal deposits. Weld J. 1982;61(4):125s–132s.
7. Gualco A, Svoboda HG, Surian ES, De Vedia L. Effect of welding procedure on wear behaviour of a modified martensitic tool steel hardfacing deposits. Mater Des. 2010; 31(9):4165–4173.
8. Francis JA. Principles for open-arc weld deposition of high-chromium white iron surface layers. Adelaide; 1999.
9. Weissmiiller J. Alloy effects in nanostructures. Nanostruct Mater. 1993;3:261–272.
10. Cullity BD, Stock SR. Elements of X-ray diffraction. 3rd ed. Prentice Hall; 2001.
11. Analysis software of Xpowder diffraction spectra, version. 2004.
12. Datasheet: TeroMatec 395NOA. Eutectic Castolin-ESAB, USA. 2008.
13. Gleiter H. Nanostructured materials: basic concepts and microstructure. Acta Mater. 2000;48(1):1–29.
14. Inoe A. Amorphous and nanocrystalline materials: preparation, properties, and applications. Springer; 2010.
15. Vaidya V. Shielding gas mixtures for semiautomatic welds. Weld J. 2002;81(9):43–48.
16. Fougere GE, Weertman JR, Siegel RW. On the hardening and softening of nanocrystalline materials. Nanostruct Mater J. 1993;3(1–6):379–384.
17. Weissmiiller J. Some basic notions on nanostructured solids. Mater Sci Eng A. 1994;179–180:102–107.
18. Morris DG. The origins of strengthening in nanostructured metals and alloys. Rev Metal. 2010;46(2):173–186.
19. Inoe A. Bulk glassy and nonequilibrium crystalline alloys by stabilization of supercooled liquid: fabrication, functional properties and applications. Part 1. Proc Jpn Acad Ser B. 2005;81.
20. Branagan DJ, Marshall MC, Meacham BE. High toughness high hardness iron based PTAW weld materials. Mater Sci Eng A. 2006;428:116–123.